A major purpose of the Technical Information Center is to provide the broadest dissemination possible of information contained in DOE's Research and Development Reports to business, industry, the academic community, and federal, state and local governments.

Although a small portion of this report is not reproducible, it is being made available to expedite the availability of information on the research discussed herein.

LA-UR -84-1538

NOTICE

PORTIONS OF THIS REPORT ARE ILLEGIBLE. It has been reproduced from the best available copy to permit the broadest possible availability.

Los Alamos National Laboratory is operated by the University of California for the United States Department of Energy under contract W-7405-ENG-36.

TITLE: SELECTION OF REGENERATOR GEOMETRY FOR MAGNETIC REFRIGERATOR APPLICATIONS

AUTHOR(S): John A. Barclay and Sunil Sarangi

SUBMITTED TO: 5th ASME/AIChE/IIR Intersociety Cryogenic Symposium, New Orleans, LA, Dec. 9-13, 1984

DISCLAIMER

Los Alamos National Laboratory
Los Alamos, New Mexico 87545

SELECTION OF REGENERATOR GEOMETRY FOR MAGNETIC REFRIGERATOR APPLICATIONS

by

John A. Barclay and Sunil Sarangi

Group P-10, MS K764

Los Alamos National Laboratory, Los Alamos, NM 87545

SELECTION OF REGENERATOR GEOMETRY FOR MAGNETIC REFRIGERATOR APPLICATIONS*

by

John A. Barclay and Sunil Sarangi

Group P-10, MS K764

Los Alamos National Laboratory, Los Alamos, NM 87545

ABSTRACT

Magnetic refrigerators that span large temperature ranges operate with regenerative cycles, such as the Brayton cycle and the Ericsson cycle. One design under investigation in our laboratory includes a pair of porous beds of magnetic material, coupled by appropriate heat transfer fluids and cycled through a magnetic field to produce refrigeration. These porous beds function both as the working material and the regenerator, and such an arrangement has been called an Active Magnetic Regenerator. It forms the heart of the refrigerator, and the efficiency of the refrigerator is critically dependent on that of the regenerator.

In our effort to develop magnetic regenerators of high efficiency we have looked at the following geometries: (a) tube channels in solid block, (b) stack of perforated plates normal to the fluid flow direction, (c) stack of solid plates parallel to fluid flow direction, and packed bed of spherical particles, (d) loose packed, and (e) sintered.

---

*Work performed under the auspices of the Department of Energy.

We report here computations of the overall efficiency of the regenerator, considering heat transfer, longitudinal conduction, and fluid pressure drop, for all the above arrangements as a function of geometrical variables, such as overall length and particle diameter or plate thickness. The results yield the optimum geometry for a given combination of other controlling parameters, such as frequency, porosity, and fluid properties. The different geometries are compared under the constraint that the mass of magnetic material is the same for all. This condition is peculiar to the magnetic refrigeration process because the net refrigeration and driving forces are proportional to the mass of magnetic material.

INTRODUCTION

Magnetic refrigeration has been the key tool in achieving temperatures below 1 kelvin. During the past few years magnetic systems have been proposed for several applications ranging between production of superfluid helium and comfort air conditioning [1-5], and are under active development in several laboratories around the world.[6,7] The refrigerator is based on the well known magnetocaloric effect [8] i.e., cooling of a magnetic material by adiabatic demagnetization. It uses paramagnetic substances for applications below 20 K and ferromagnetic materials near their respective Curie temperatures at higher temperatures. The thermodynamic process is based on a common cycle: Carnot, Stirling, Ericsson, or Brayton. The material is magnetized in thermal communication with the high temperature sink and demagnetized in contact with the low temperature source. The two steps may be linked by two adiabatic processes, giving a Carnot cycle, the temperature range being limited to the adiabatic temperature change. The range can be extended to many times this value by suitable regenerators or heat exchangers.

One design under investigation in our laboratory for application to liquefaction of hydrogen (77-20 K) uses a porous bed of ferromagnetic materials which functions both as the working material and as the regenerator coupled to the source and the sink by circulating helium gas. Such an arrangement has been called an active magnetic regenerator (AMR) [9,10].

ACTIVE MAGNETIC REGENERATOR

Consider a porous bed regenerator composed of a series of different ferromagnetic materials with Curie temperatures T_o gradually decreasing from the sink temperature T_h to the load temperature T_c. The initial temperature profile is shown in frame I of Fig. 1. Upon application of a magnetic field the temperature along the bed increases by an amount ΔT which is a function of the local absolute temperature T.

In real materials the absolute temperature T, the adiabatic temperature change $\Delta T(1)$, the isothermal entropy change $\Delta S(T)$ and specific heat C(T) are related in a rather complex manner. For lowest thermodynamic irreversibility we have assumed that ΔS is constant over the entire temperature range and that the adiabatic temperature change ΔT is proportional to the absolute temperature T. Then,

$$\frac{\Delta T_h}{\Delta T_c} = \frac{T_h}{T_c} \quad , \tag{1}$$

the subscripts h and c referring to the hot and cold ends, respectively. These assumptions simplify considerably the computations affecting all the geometries to the same extent.

The matrix temperature profile on magnetization is shown in frame II of Fig. 1. With the material still inside the magnetic field, pressurized helium

or hydrogen gas at temperature T_c is pushed through the bed from the cold end, cooling the entire bed near to its original state (frame III). The gas, on the other hand, leaves at a temperature $T_h + \Delta T_h$ at the beginning of this step reducing to T_h at the end, the average exit temperature being $T_h + \phi_h \Delta T_h$; $0 < \phi_h < 1$. The field is now removed isentropically. The bed cools by $\Delta T(T)$, identical to the amount of heating during magnetization process. The resulting temperature profile is shown in frame IV. The cold end is now at a temperature $T_c - \Delta T_c$ which is below the load temperature. The gas flow is now reversed and gas at sink temperature is blown over the bed from the warm end. The bed warms up to its original state (frames V and I). The fluid exit temperature remains between $T_c - \Delta T_c$ and T_c, with an average $T_c - \phi_c \Delta T_c$; $0 < \phi_c < 1$. ϕ_h and ϕ_c can be determined only by a detailed simulation of the refrigeration cycle [9]. In this paper both ϕ_h and ϕ_c are assumed to be 0.75. The cold gas carries with it the net refrigeration power with an average rate of $\dot{m}_f c_p \phi_c \Delta T_c$, where $\dot{m}_f$ is the mass flow rate of the gas and c_p its specific heat. Two identical AMR units operate in opposite phase to provide continuous refrigeration.

The heat transfer mechanism in the AMR is same as that in an ordinary thermal regenerator except for the step changes in temperature created by the application and removal of the magnetic field. The COP of the refrigerator is strongly dependent on the effectiveness of the regenerator. Hence an AMR must have a high effective N_{tu} for successful operation of the magnetic refrigerator.

THE OPTIMIZATION PROBLEM

It is necessary to achieve the maximum possible N_{tu} with the given amount of magnetic material. This is done by selecting the optimum geometry and the optimum dimensions. The techniques of surface selection and optimization of

geometric parameters in compact heat exchangers have been discussed by several authors. [11-13] Shah [11] has summarized over 30 different methods of comparing compact heat exchanger surfaces. These methods are limited to only one side of a compact heat exchanger. This objection is not relevant in the case of a magnetic regenerator where there is only one surface and the two streams are identical. On the other hand, these methods consider only the losses associated with finite heat transfer coefficient and viscous pressure drop and do not take into account such effects as longitudinal conduction in the bed and gas dispersion. The two latter sources can be significant in high N_{tu} regenerators.

The optimization of physical dimensions has been discussed by Shah et al. [12]. They have described several search techniques which have been successfully applied to heat exchanger optimization. In our case the parameter space is limited and it was felt that sophisticated search techniques may be avoided in favor of a simple program covering the entire parameter space

An alternative method of surface selection and optimization is provided by the second law analysis.[13] The aim in this technique is to minimize the entropy generation rate in a thermal system.

The total entropy generation rate $\dot{S}$ may be considered to be the sum of 3 terms.

$$\dot{S} = \dot{S}_1 + \dot{S}_2 + \dot{S}_3 \tag{2}$$

where

$$\dot{S}_1 = \frac{\dot{q}_r}{N_{tu} + 1} \left(\frac{1}{T_c} - \frac{1}{T_h} \right) , \tag{3}$$

is the entropy generation rate due to finite heat transfer coefficient, $\dot{q}_r$ being the heat transfer rate in the regenerator;

$$\dot{S}_2 \simeq \frac{\dot{V}_f \Delta P}{T_h} \tag{4}$$

is the entropy generation rate due to viscous dissipation of energy, $\dot{V}_f$ being the average volume flow rate and ΔP the pressure drop across the bed;

and $$\dot{S}_3 \simeq \frac{\lambda A_c}{L} \frac{(T_h - T_c)^2}{T_h T_c} \quad , \tag{5}$$

is the entropy generation rate due axial conduction and gas dispersion along the bed, λ being the effective thermal conductivity, L the length, and A_c the cross sectional area. In the search for the optimum geometry S is the objective function to be minimized under the constraints imposed by manufacturing difficulties, and the size and cost of the magnet system.

The entropy generation rate $\dot{S}$ is equivalent to loss of available energy at the rate [13] $T_h\dot{S}$. The power required for a refrigeration load $\dot{q}_c$ at temperature T_c is then,

$$\dot{W} = \dot{q}_c\left(\frac{T_h}{T_c} - 1\right) + T_h\dot{S} \tag{6}$$

The inefficiencies due to all other sources such as pumps, drive system, hot and cold end heat exchangers, and heat transfer from the ambient which are not directly dependent on regenerator geometry have been neglected. A figure of merit (FOM) for the refrigerator can now be defined as:

$$\text{FOM} = \frac{\text{Ideal (Carnot) power required}}{\text{Actual power required}} = \frac{\dot{q}_c\left(\frac{T_h}{T_c} - 1\right)}{\dot{q}_c\left(\frac{T_h}{T_c} - 1\right) + T_h\dot{S}} \tag{7}$$

The minimum entropy generation rate corresponds to the highest figure of merit. In this paper we have used the FOM as defined above as the objective function for optimization of regenerator geometry.

THE PARAMETER SPACE

We have considered the following geometries for the regenerator (Fig. 2).

(a) tube channels in solid block,

(b) a stack of perforated plates separated by small spacers normal to the fluid flow direction,

(c) stack of solid plates parallel to fluid flow direction,

(d) packed bed of spherical particles: loose packed, and

(e) packed bed of spherical particles: sintered.

The geometries (a), (c), (d), and (e) are characterized by 3 parameters:

(i) overall length L

(ii) overall porosity α

(iii) characteristic dimension (hole diameter d, particle diameter d_p, or plate thickness t)

The perforated plate geometry, however, needs more dimensions:

(i) overall length L,

(ii) overall porosity α,

(iii) plate thickness t,

(iv) hole diameter d,

(v) plate spacing s.

In each case the volume of magnetic material is constant. Table 1 summarizes the effects of variation of these parameters on the three sources of entropy generation, the other dimensions being assumed constant.

T .e 1

Geometry	Change of entropy due to → with increase in→	Heat Transfer $\dot{S}_1$	Pressure Drop $\dot{S}_2$	Axial Conduction $\dot{S}_3$
(a-e)	overall length L	decreases slowly	increases	decreases
(a-e)	overall porosity α	decreases	decreases	nearly unchanged
a,b	hole diameter d	increases	decreases	nearly unchanged
b	plate thickness t	increases slowly	decreases slowly	nearly unchanged
b	relative plate spacing s/t	increases	increases	decreases
c	plate thickness t	increases	decreases	nearly unchanged
d,e	particle diam d_p	increases	decreases	increases

For all the parameters except the overall porosity α, the three sources of irreversibility compete among each other suggesting an optimum for the dimension. On the other hand, the overall entropy generation rate decreases monotonically with increase in overall porosity. Increased porosity at constant material volume results in increased total volume, requiring a correspondingly larger magnet which offsets the gain in regenerator efficiency. In this paper the different geometries have been compared keeping the overall porosity fixed at 40%, which is the porosity of a randomly packed bed of spherical particles.

In addition to the above, the following dimensional constraints are imposed by manufacturing limitation and to avoid unwieldy geometries. d, t, s, d_p, a and L refer to hole diameter, plate thickness, plate spacing, particle diameter, and overall width length of the bed, respectively.

(a) tube channels in solid block: $0.010 \text{ mm} < d < 1 \text{ mm}$,

(b) stack of perforated plates normal to fluid flow direction:

$0.010 \text{ mm} < d < 1.0 \text{ mm}$

$0.010 \text{ mm} < t < 1.0 \text{ mm}$

$0.2 < s/t < 0.6$

(c) stack of solid plates parallel to fluid flow direction:

$0.010 \text{ mm} < t < 1.0 \text{ mm}$

(d) and (e) packed bed of spherical particles:

$0.010 \text{ mm} < d_p < 1 \text{ mm}$

The aspect ratio $\beta = L/a$ is limited between 0.3 and 30 for all geometries.

CALCULATION OF ENTROPY GENERATION RATES

The inputs to the problem are the temperatures: T_h, T_c; the refrigeration load: $\dot{q}_c$; magnetocaloric properties of the matrix material: ΔT_c and ΔS, density ρ_m, specific heat c_m, and thermal conductivity κ_m; physical and transport properties of the fluid: ρ_f, c_p, μ, κ_f at the average temperature $(T_h + T_c)/2$. The operating frequency ν is a parameter which is varied between 0.1 Hz and 10 Hz. At lower frequencies the volume of the regenerator and hence that of the magnet system is high, and at higher frequencies eddy current and hysteresis losses generate heat in the regenerator. The following relations are used to determine the entropy generation rates from the input parameters given above.

The required fluid flow rate to convey refrigeration load $\dot{q}_c$ at an average temperature change of $\phi_c \Delta T_c$ is

$$\dot{m}_f = \frac{\dot{q}_c}{c_p \phi_c \Delta T_c} \tag{8}$$

and the corresponding volume flow rate

$$\dot{V}_f = \dot{m}_f / \rho_f \tag{9}$$

The fluid undergoes a total temperature change of $T_h - T_c$ in the regenerator. Then the rate of heat transfer in the regenerator

$$\dot{q}_r = \dot{m}_f c_p (T_h - T_c) = \frac{\dot{q}_c (T_h - T_c)}{\phi_c \, \delta T_c} \tag{10}$$

The volume of magnetic material, the total volume including the voids and the cross sectional area are related to $\dot{q}_r$ as:

$$V_m = (1-\alpha) V_T = (1-\alpha) L A_c = \frac{\dot{q}_r}{\nu \, \Delta S \, (T_h + T_c)/2} \tag{11}$$

where ν is the operating frequency and ΔS the isothermal entropy change of the material per unit volume.

The hydraulic diameter and Reynolds number for a given geometry are given as

$$d_h = \frac{4V_T}{A} \quad \text{and} \quad N_R = \frac{\dot{m} \, d_h}{\alpha A_c \mu} \quad , \tag{12}$$

A being the total heat transfer area. In appendix A the relevant correlations have been listed which determine Nussult number ($N_{Nu} = h d_h / \kappa_f$) and friction factor f from Reynolds number N_R and Prandtl number N_{Pr}. The pressure drop ΔP and the number of heat transfer units N_{tu} can now be determined by the relations

$$\Delta P = \frac{4 f L \dot{m}^2}{2 \rho \, d_h \, A_c^2} \quad \text{and} \quad N_{tu} = \frac{hA}{\dot{m} c_p} \tag{13}$$

These values are substituted in Eqs. (2), (3), (4), (5), and (7), to determine the objective function FOM for a given set of geometric parameters: aspect

ratio β and the characteristic dimensions such as hole diameter d, plate thickness t, relative plate spacing s/t, or particle diameter d_p. The set of geometric parameters are now varied over the parameter space. The configuration where the entropy generation rate is minimum gives the optimum geometry for given frequency and porosity.

RESULTS AND DISCUSSION

Figures of merit computed over the parameter space described earlier have been plotted as contour diagrams against aspect ratio β and a characteristic dimension d, t, or d_p. Some of these contour plots have been given in Figs. (3-7). We have found that such contour plots on log-log scales generated by standard algorithm is a very convenient and powerful technique to represent heat exchanger calculations and to arrive at optimum geometries. Optimum values of aspect ratio and characteristic dimensions along with the corresponding FOMs have been presented in Table 2 for selected frequencies.

In the case of perforated plate geometry, results have been presented for plate thickness t = 0.50 mm and relative plate spacing s/t = 0.2 and 0.4. Calculations with t = 0.25 mm and t = 1.0 mm show negligible effect of plate thickness if other parameters are kept constant. Relative spacing s/t = 0.6 yields very low FOM. Because the total void fraction is constant at 0.4, at high values of s/t, the void space associated with the holes is reduced significantly. This reduces the heat transfer area and consequently the FOM.

The optimum FOM is highest for the perforated plate geometry, but is nearly as high for tube channels and solid plates geometries. The optimum aspect ratios and hole diameters are, however, quite different. Packed beds are characterized by little lower FOM; but they are favored by lower cost and simplicity of construction.

It may be observed that lower frequency yields higher efficiency. This is because the amount of magnetic material increases at lower frequency, providing higher heat transfer area and flow cross section. The optimum dimensions, however, are strongly dependent on the frequency, which should be taken into account in design.

Table 2

CONFIGURATIONS FOR MAXIMUM FIGURE OF MERIT AT SELECTED VALUES OF FREQUENCY AND OTHER PARAMETERS

(a) Tube channels in solid block

Frequency Hz	Aspect Ratio B	Hole Diameter d (mm)	FOM
0.1	18.93	0.251	0.948
1.0	5.99	0.126	0.895
10.0	1.89	0.063	0.797

(b) Stack of perforated plates (t=0.50 mm) normal to the direction of fluid flow

	relative plate spacing s/t = 0.2			relative plate spacing s/t = 0.4		
Frequency	B	d (mm)	FOM	B	d (mm)	FOM
0.0	4.75	0.158	0.969	3.00	0.126	0.963
1.0	1.50	0.079	0.936	0.95	0.063	0.923
10.0	0.48	0.032	0.873	0.30	0.025	0.852

(c) Stack of solid plates parallel to the fluid flow direction

Frequency Hz	Aspect ratio B	Plate thickness t (mm)	FOM
0.1	18.93	0.251	0.952
1.0	5.99	0.126	0.902
10.0	2.38	0.063	0.809

(d) Packed bed of spherical particles

	Loose Packed			Sintered		
Frequency Hz	B	d_p (mm)	FOM	B	d_p	FOM
0.1	9.49	0.631	0.909	11.94	0.794	0.908
1.0	3.00	0.316	0.823	3.78	0.398	0.820
10.0	0.95	0.126	0.683	1.19	0.158	0.679

REFERENCES

1. Brown, G. V., "A Magnetic Heat Pump Near Room Temperatures," J. Appl. Phys. 47, 3673-80 (1976).
2. Steyert, W. A., "Stirling-cycle Rotating Magnetic Refrigerators and Heat Engines for Use Near Room Temperature," J. Appl. Phys. 49, 1216-26 (1978).
3. Barclay, J. A., "Can Magnetic Refrigerators Liquefy Hydrogen at High Efficiency?" ASME paper No. 81-HT-82 (1981).
4. Barclay, J. A., Moze, O., and Paterson, L., "A Reciprocating Magnetic Refrigerator for 2-4 K Operation: Initial Results," J. Appl. Phys. 50(9), 5870-77 (1979).
5. Barclay, J. A., "Magnetic Refrigeration for Spacecraft Systems," ASME paper 81-ENAs-47 (1981).
6. Lacaze, A. F., et al., "Double Acting Reciprocating Magnetic Refrigerator: Recent Improvements," paper BA-2, Cryogenic Engineering Conference, Boulder, Colorado, Aug. 15-19, 1983.
7. Nakagome H., et al., "The Helium Magnetic Refrigerator I: Development and Experimental Results," paper FC-10, Cryogenic Engineering Conference, Boulder, Colorado, Aug. 15-19, 1983.
8. Hudson, R. P., Principles and Applications of Magnetic Cooling, North Holland (1972).
9. Barclay, J. A., "The Theory of an Active Magnetic Regenerative Refrigerator," in Refrigeration for Cryogenic Sensors, M. Gasser (Ed), NASA Conference Publication 2287 (1983) p. 375-87.
10. Barclay, J. A. and Steyert, W. A., "Active Magnetic Regenerator," U.S. Patent No. 4,332,135 (1982).
11. Shah, R. K., "Compact Heat Exchanger Surface Selection Methods," Proceedings of the 6th International Heat Transfer Conference, Toronto, Canada, Vol. 4, 193-99 (1978).

12. Shah, R. K., Afimiwala, K. A., and Mayne, R. W., "Heat Exchanger Optimization, Proceedings of the 6th International Heat Transfer Conference, Toronto, Canada, Vol. 4, 185-91 (1978).

13. Bejan, A., "Second Law Analysis in Heat Transfer and Thermal Design," in Advances in Heat Transfer, J. P. Hartnett and T. F. Irvine Jr., (Eds.), Vol. 15, p. 1-58 (1982).

14. Rohsenow, W. M. and Hartnett, J. P., Handbook of Heat Transfer, McGraw Hill (1973), Chapter 7.

15. Fleming, R. B., "A Compact Perforated Plate Heat Exchanger," in Advances in Cryogenic Engineering, K. D. Timmerhaus (Ed.), Plenum Press, 14, 197-204 (1968).

16. Kays, W. M. and London, A. L., Compact Heat Exchangers, McGraw Hill (1964).

17. Macdonald, I. F., et al., "Flow Through Porous Media - the Ergun Equation Revisited," Ind. Eng. Chem. Fundam. 18, 199-208 (1979).

18. Coppage, J. E. and London, A. L., "Heat Transfer and Flow Friction Through Porous Media," Chem. Eng. Progress 52(2), 57-F - 63-F (1956).

19. Beveridge, G. S. G. and Haughey, D. P., "Axial Heat Transfer in Packed Beds: Stagnant Beds Between 20 and 750°C," Int. J. Heat Mass Transfer 14, 1093-1113 (1971).

20. Edwards, M. F. and Richardson, J. F., "Gas Dispersion in Packed Beds," Chem. Eng. Sc. 23, 109-23 (1968).

APPENDIX A

CORRELATIONS USED IN PREDICTING NUSSELT NUMBERS AND FRICTION FACTORS FOR VARIOUS GEOMETRIES

(a) Solid block with longitudinal holes.[14]

Laminar flow ($N_R < 2200$):

$$f = 16/N_R \tag{A1}$$

$$N_{Nu,H} = 4.364 \tag{A2}$$

Turbulent Flow ($N_R > 4400$)

$$f = 0.071\ N_R^{-0.25} \tag{A3}$$

$$N_{Nu,H} = 0.022\ N_R^{0.8}\ N_{Pr}^{0.6} \tag{A4}$$

In the transition flow regime ($2200 < N_R < 4000$) the flow is unstable and the friction factor and Nusselt number are generally uncertain. In actual design this regime is normally avoided. For the sake of comparison between different geometries and to avoid numerical errors we adopt the following interpolation between the laminar and turbulent flow expressions.

$$f = [16/N_R(4000 - N_R) + 0.071\ N_R^{-0.25}\ (N_R - 2200)]/1800 \tag{A5}$$

and $N_{Nu,H} = [4.364\ (4000 - N_R) + 0.022\ N_R^{0.8}\ Pr^{0.6}\ (N_R - 2200)]/1800$

The effective axial conductivity

$$\lambda = (1-\alpha)\ \kappa_m \tag{A7}$$

where κ_m is the thermal conductivity of the solid and α the porosity.

(b) Perforated plates normal to fluid flow direction:

Following Ref. [15] we have considered heat transfer only in the cylindrical walls of the perforations, ignoring the front and back faces of the plates. The actual performance is expected to be somewhat better due the contribution of these surfaces. Because the length of these

cylindrical passages (= thickness of the plates) is comparable to the diameter, entrance region correlations are to be used.

Laminar regime ($N_R < 2200$)

$$f = \frac{16}{N_R} \quad \text{for} \quad N_R \frac{d}{t} < 10 \tag{A8}$$

$$\text{and} \quad f = 3.492 \left(\frac{d}{t}\right)^{.661} N_R^{-.339} \quad \text{for} \quad N_R \frac{d}{t} > 10 \tag{A9}$$

$$N_{Nu,H} = 4.364 \quad \text{for} \quad N_R N_{Pr} \frac{d}{t} < 6.667 \tag{A10}$$

$$\text{and } N_{Nu,H} = 2.347 \left(N_R N_{Pr} \frac{d}{t}\right)^{.3265} \text{ for } N_R N_{Pr} \frac{d}{t} > 6.667 \tag{A11}$$

The above correlations have been obtained by fitting suitable expressions to experimental data given in Ref. [16].

The turbulent regime ($N_R > 4000$) correlations given in Eqs. (A3) and (A4) are used. Correlations in the transition regime may be derived by interpolation between Eqs. (A9) and (A3) and between (A11) and (A4) in a manner similar to that used in the derivation of Eqs. (A5) and (A6).

Let us further assume that the spacers are made of the same material as the plates and occupy 1% of the cross sectional area. Then the system may be described as a bed of cross sectional area ($A_c - n\pi d^2/4$) and length Nxt in series with one of cross sectional area 0.01 A_c and length (N-1)s, N being the number of plates. The effective thermal conductivity of this sytem is, then,

$$\lambda = \kappa_m L \Bigg/ \left(\frac{N t A_c}{A_c - n\pi d^2/4} + \frac{(N-1)s}{0.01} \right) \tag{A12}$$

(c) Stack of solid plates parallel to fluid flow direction. [14]

Laminar flow ($N_R < 2200$)

$$f = 24/Re \tag{A13}$$

$$N_{Nu,H} = 8.235 \tag{A14}$$

Turbulent flow ($N_R > 4000$)

$$f = 0.071\ N_R^{-0.25} \tag{A15}$$

$$N_{Nu,H} = 0.021\ N_R^{0.8}\ N_{Pr}^{0.6} \tag{A16}$$

Equation (A16) has been obtained by fitting an equation of the form: $N_{Nu,H} = A\ N_R^{0.8}\ N_{Pr}^{0.6}$ to experimental data given in Ref. [14].

In the transition flow regime f and $N_{Nu,H}$ are determined in a manner similar to that used for Eqs. (A5) and (A6). The effective axial conductivity is given by the relation,

$$\lambda = (1-\alpha)\,\kappa_m \tag{A17}$$

(d) Packed bed of spheres: loose packed, and

(e) Packed bed of spheres: sintered.

The pressure drop in packed bed of spherical particles can be represented by the well known Ergun equation as modified by Macdonald et al. [17] and the heat transfer correlation is given by Coppage and London [18] in terms of Reynolds number.

$$f' = 180\ \frac{1-\alpha}{N_R'} + 1.80$$

$$\text{with}\quad N_R' = \frac{\dot{m}\, d_p}{\mu\, A_c} \quad \text{and} \quad f' = \frac{\Delta P\ \rho\ A_c^2\ d_p\ \alpha^3}{\dot{m}^2\ L\ (1-\alpha)} \tag{A18}$$

$$N_{Nu,H} = 0.21\ N_R^{\,0.69}\ , \tag{A19}$$

N_R being defined in Eq. (11). The problem of axial conduction in packed beds has been discussed in Ref. [19].

$$\frac{\lambda}{\lambda_f} = \varepsilon_{A1} + \left(\frac{1 - \psi}{\frac{\kappa_m}{\lambda_f}\left(1 - \varepsilon_{A1}\right)} + \frac{\psi}{\varepsilon_{A2} + \frac{\kappa_m}{\lambda_f}\,\varepsilon_{A3}} \right)^{-1} \tag{A20}$$

ε_{A1}, ε_{A2}, and ε_{A3} are fractions of cross sectional area devoted to fluid-fluid, fluid-solid, and solid-solid conduction path. For a randomly packed bed (α = 0.40) the following values have been estimated [19]. $\varepsilon_{A1} = 0.3076$; $\varepsilon_{A2} + \varepsilon_{A3} = .6924$ and $\psi\ \varepsilon_{A2} = 0.09245$. The fraction of cross section devoted to solid-solid conduction, ε_{A3} is difficult to determine without some experiment. We have chosen $\varepsilon_{A3} = 0.001$ for loose packed and $\varepsilon = .05$ for sintered bed.

κ_m is the solid conductivity and is a material property. λ_f, on the other hand, signifies the effective axial conductivity in the fluid due to gas conduction and gas dispersion. Edwards and Richardson [20] have investigated the gas dispersion problem in packed beds. Their results may be expressed as:

$$\lambda_f = \kappa_f \text{ for } N_R' < 2\,\alpha/N_{Pr}$$

$$\text{and } \lambda_f = \frac{m_f\, c_p\, d_p}{2\, A_c\, \alpha} \text{ for } N_R' > 2\,\alpha/N_{Pr}$$

NOMENCLATURE

a = width of bed (square cross section)

A = a constant

A = heat transfer area (m^2)

A_c = cross sectional area of bed (m^2)

c_m = specific heat of matrix material

c_p = specific heat of fluid at constant pressure (J/kg K)

d = diameter of holes (m)

d_p = diameter particles (m)

d_h = hydraulic diameter (m)

f = friction factor

f' = friction factor in packed bed of spheres

h = heat transfer coefficient (W/m^2 K)

L = length of bed (m)

$\dot{m}$ = fluid flow rate through the bed (kg/s)

n = number of holes

n_p = number of particles in packed bed

N = number of plates

$N_{Nu,H}$ = Nusselt number at constant heat ransfer rate

$= hd/k_f$

N_{Pr} = Prandtl number = $c_p \mu / k_f$

N_R = Reynolds number based on real fluid velocity and hydraulic diameter

N'_R = Reynolds number based on empty column velocity and particle diameter

N_{tu} = number of heat transfer units

P = pressure (N/m^2)

$\dot{q}_c$ = refrigeration load (W)

$\dot{q}_r$ = heat transfer rate in regenerator (W)

s = plate spacing (m)

$\dot{S}$ = total entropy generation rate (W/K)

$\dot{S}_1$ = entropy generation rate due to finite heat transfer coefficient (W/K)

$\dot{S}_2$ = entropy generation rate due to viscous dissipation of energy (W/K)

$\dot{S}_3$ = entropy generation rate due to axial heat conduction (W/K)

t = plate thickness (m)

T = temperature (K)

$\dot{V}_f$ = volume flow rate of fluid (m^3/s)

V_m = volume of magnetic material (m^3)

V_T = total bed volume (m^3)

α = porosity

β = aspect ratio = L/a

ΔS = isothermal entropy change ($J/K\ m^3$)

ΔT = adiabatic temperature change (K)

ε_{A1} = fraction of cross sectional area devoted to fluid-fluid conduction

ε_{A2} = fraction of cross sectional area devoted to fluid-solid conduction

ε_{A3} = fraction of cross sectional area devoted to solid-solid conduction

ϕ = a number between 0 and 1 defined in text

κ = thermal conductivity (W/mK)

λ = effective thermal conductivity of bed (W/mK)

λ_f = effective thermal conductivity of fluid (W/mK)

μ = viscosity (kg/ms)

ρ = density (kg/m^3)

Ψ = parameter used in deriving effective axial conductivity

Subscripts

c = cold end

c = cross section

f = fluid

h = hot end

m = magnetic material

r = regenerator

T = total

FIGURE CAPTIONS

Fig. 1. Temperature profiles during various steps in the operation of an AMR refrigerator. The broken lines in frames II and IV indicate the initial state.

Fig. 2. Regenerator geometries: (A) solid block with longitudinal holes, (B) stack of perforated plates normal to fluid flow direction, (C) stack of solid plates parallel to fluid flow direction, and (D) packed bed of spherical particles, loose or sintered. In our analysis sides a and b are equal.

Figs. 3., 4., 5., 6., 7a., 7b., 7c. Contour diagrams showing figure of merit against aspect ratio (x-axis) and characteristic dimension (y-axis) for different geometries.

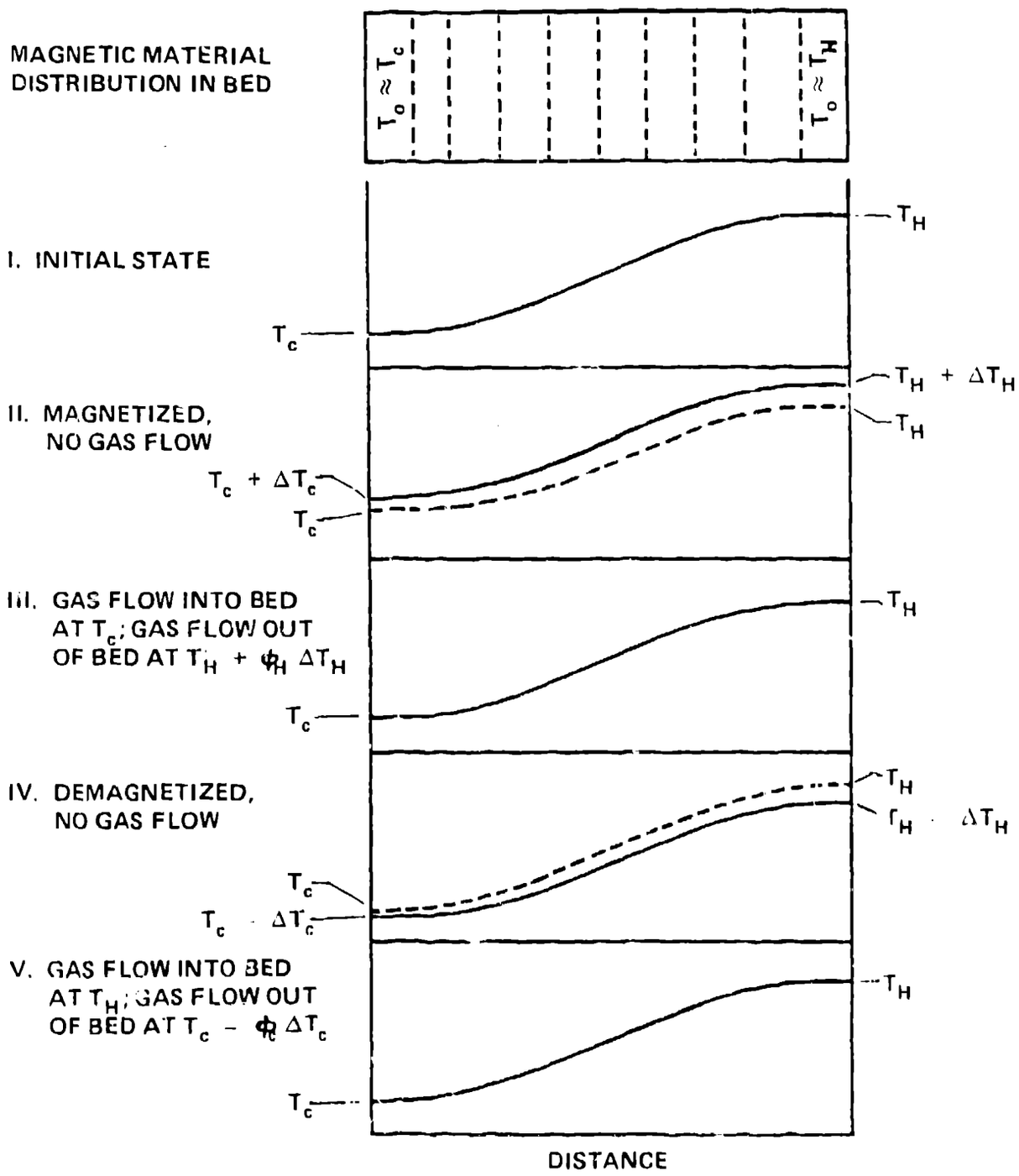
MAGNETIC MATERIAL DISTRIBUTION IN BED
$T_o \approx T_c$
$T_o \approx T_H$
I. INITIAL STATE
T_H
T_c
II. MAGNETIZED, NO GAS FLOW
$T_H + \Delta T_H$
T_H
$T_c + \Delta T_c$
T_c
III. GAS FLOW INTO BED AT T_c; GAS FLOW OUT OF BED AT $T_H + \Phi_H \Delta T_H$
T_H
T_c
IV. DEMAGNETIZED, NO GAS FLOW
T_H
$T_H - \Delta T_H$
T_c
$T_c - \Delta T_c$
V. GAS FLOW INTO BED AT T_H; GAS FLOW OUT OF BED AT $T_c - \Phi_c \Delta T_c$
T_H
T_c
DISTANCE

Fig 1.

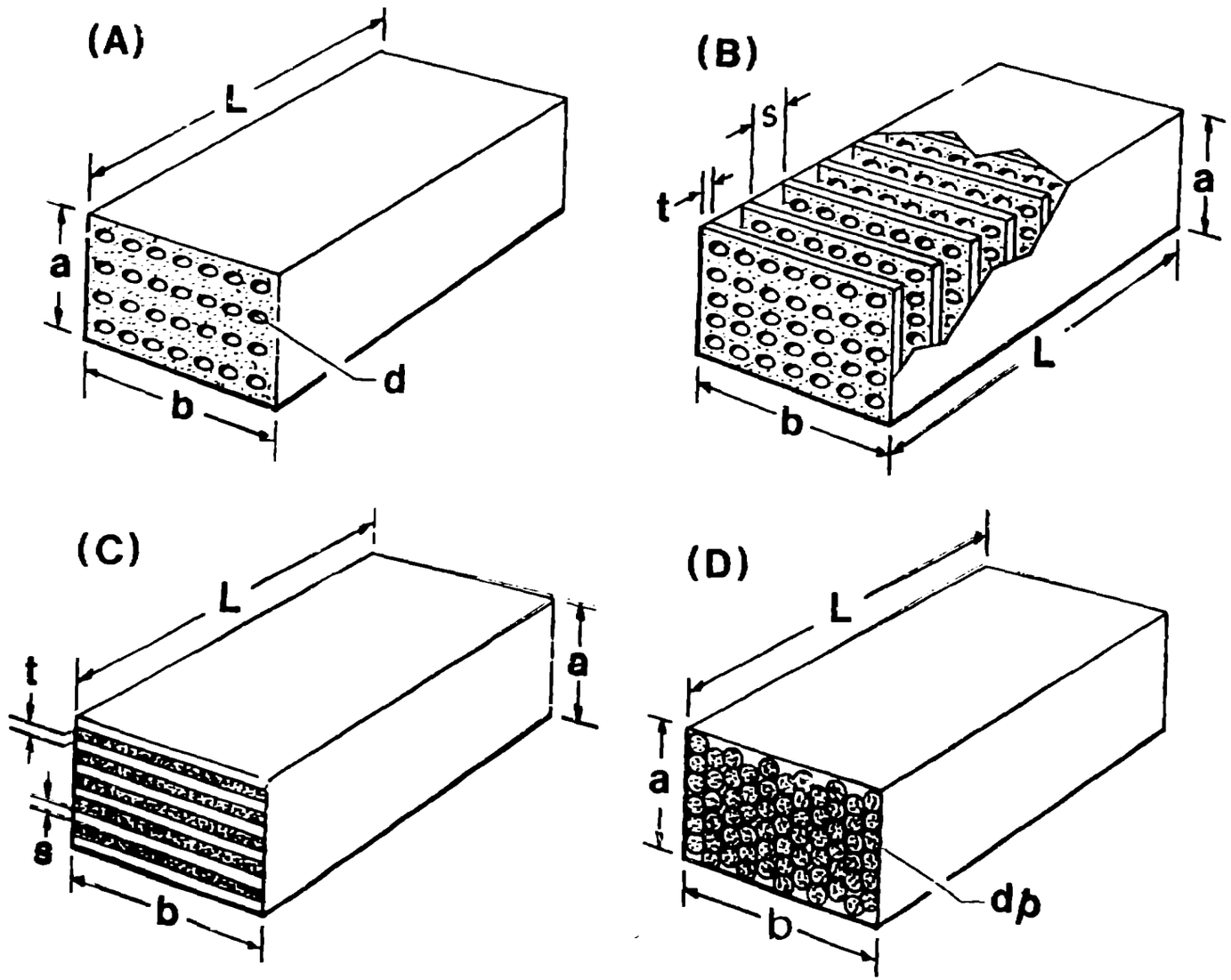

Fig 2

0.3
1
10
0.69
TUBE CHANNELS IN SOLID BLOCK
X-AXIS=ASPECT RATIO Y-AXIS=HOLE DIA
FREQUENCY= 1.0HZ

Fig. 3

PARALLEL PLATES GEOMETRY
X-AXIS=ASPECT RATIO Y-AXIS=PLATE THICKNESS
FREQUENCY = 1.0HZ
0.90
0.3
1
10

Fig. 4

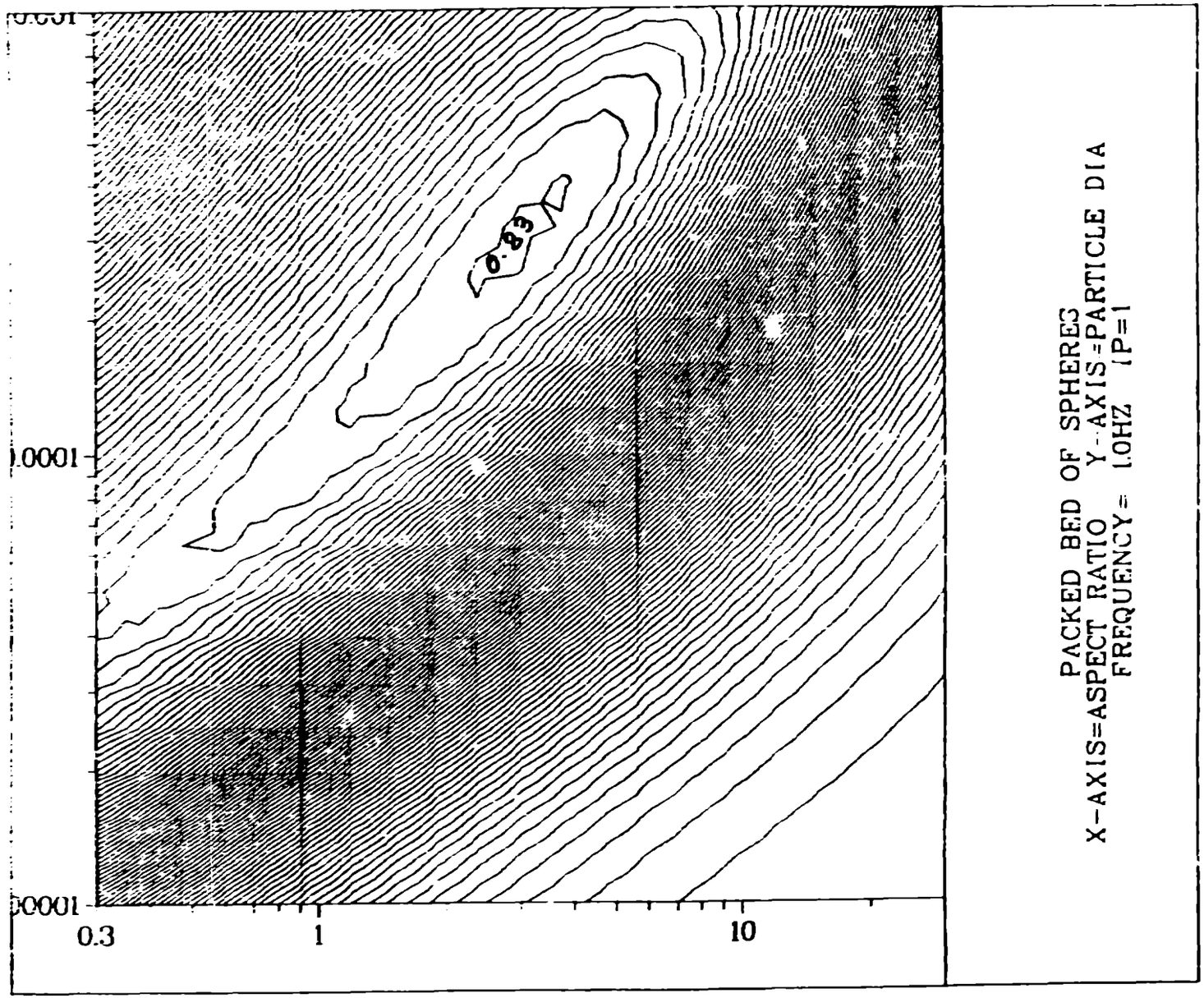
PACKED BED OF SPHERES
X-AXIS=ASPECT RATIO Y-AXIS=PARTICLE DIA
FREQUENCY= 1.0HZ IP=1
0.83
.0001
0001
0.3
1
10

Fig. 5

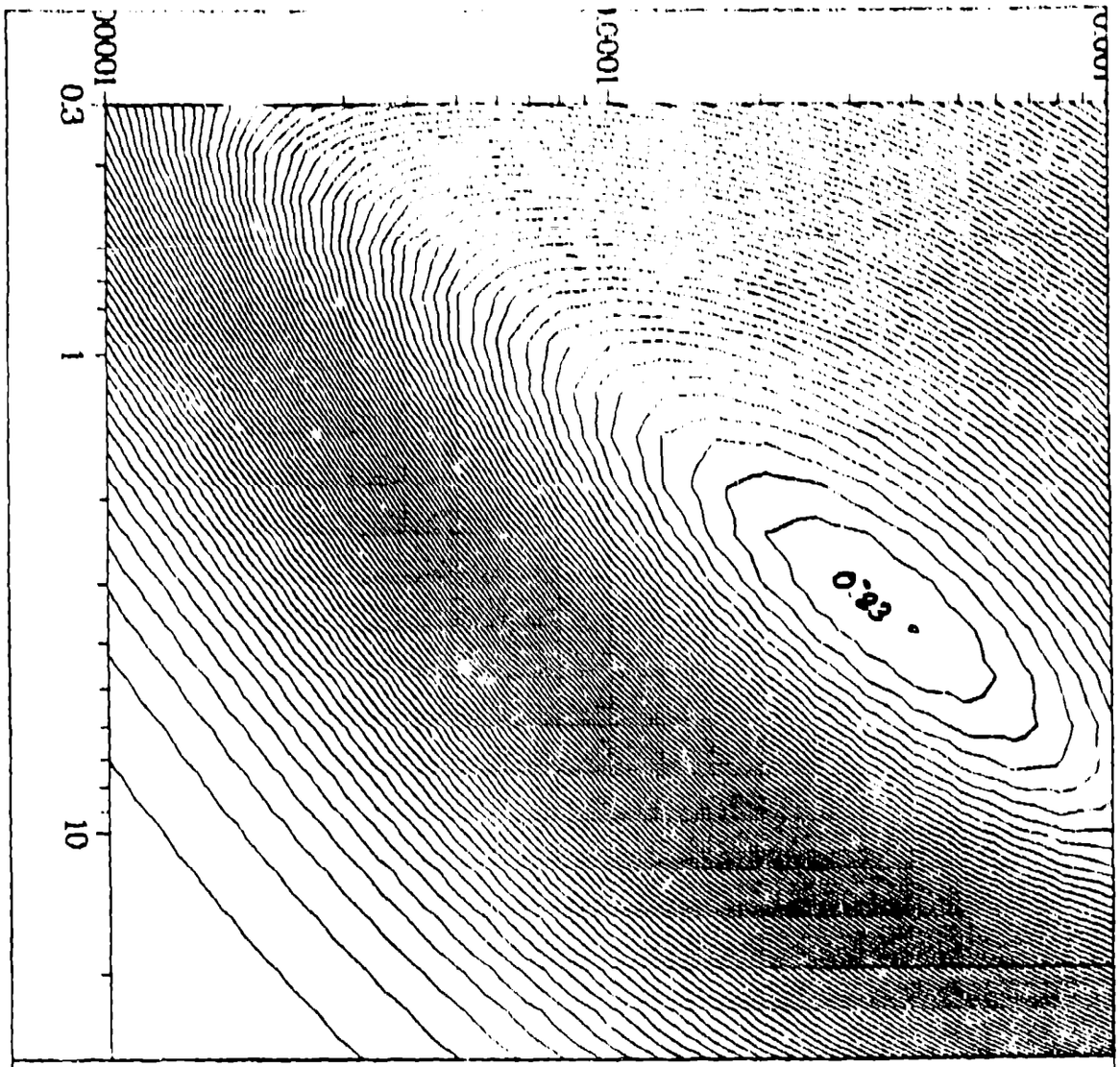

PACKED BED OF SPHERES
X-AXIS=ASPECT RATIO Y-AXIS=PARTICLE DIA
FREQUENCY = 1.0HZ IP=2

PERFORATED PLATES
X-AXIS=ASPECT RATIO Y-AXIS=HOLE DIA
FREQUENCY= 10HZ T- 50MM S T- 2
FIRST THICK CONTOUR ETA-0.85
0.93
0.03
1
10

Fig

0.3
1
10
0.93
FIRST THICK CONTOUR DIA=0.85
PERFORATED PLATES
X-AXIS=ASPECT RATIO Y-AXIS=HOLE DIA
FREQUENCY- 10HZ T= 500MM S T- 4

Fig 7

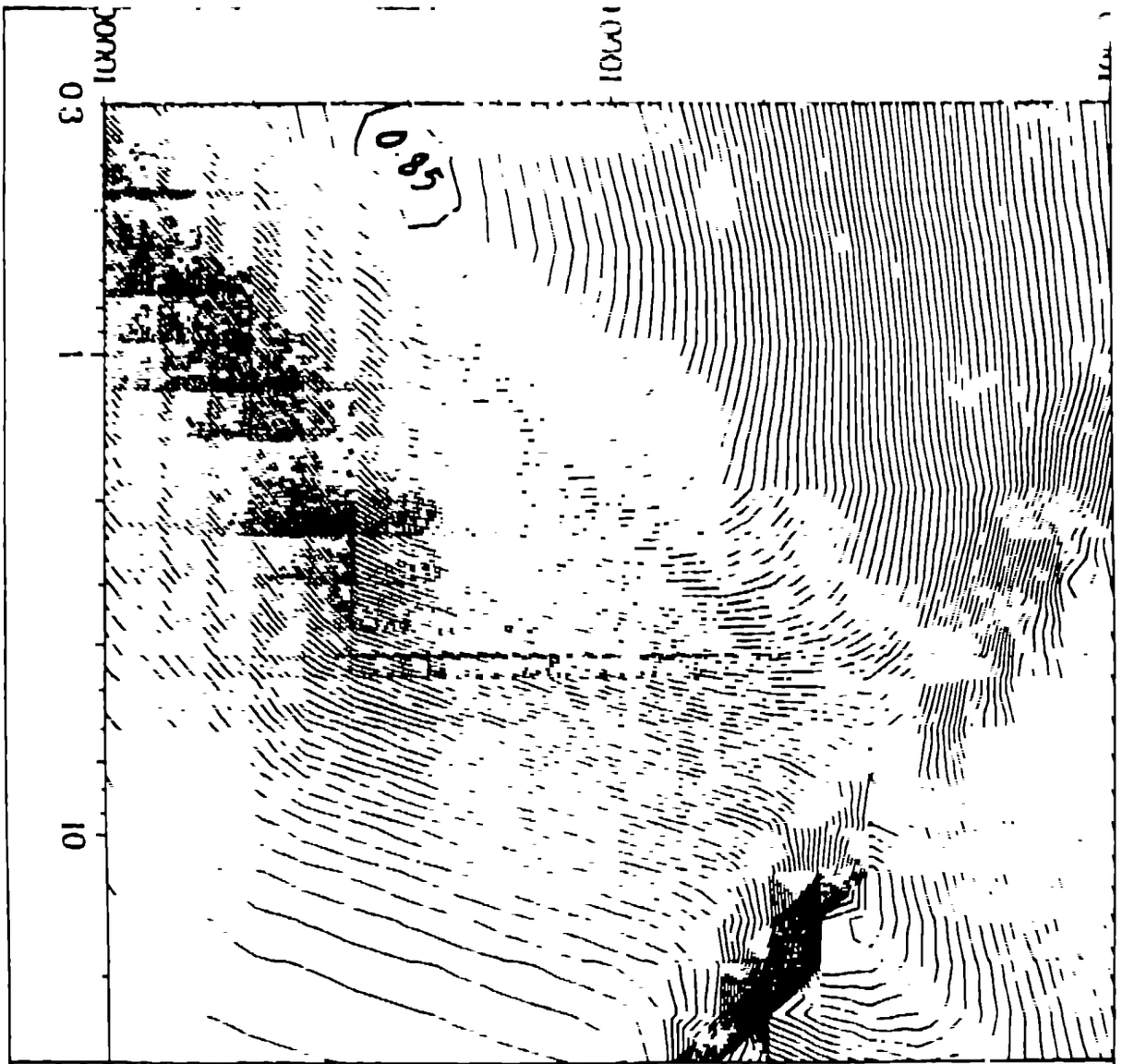
0.85
FIRST THICK CONTOUR ETA=0.85
PERFORATED PLATES
X-AXIS=ASPECT RATIO Y-AXIS=HOLE DIA
FREQUENCY= 10HZ L= 500MM S T= 6

Fig 7